The effect of faults on the 3D connectivity of reservoir bodies: a case study from the East Pennine Coalfield, UK

W. R. Bailey[1], T. Manzocchi[1], J. J. Walsh[1], K. Keogh[2,5], D. Hodgetts[2], J. Rippon[3], P. A. R. Nell[1,4], S. Flint[2] and J. A. Strand[1]

[1]*Fault Analysis Group, Department of Geology, University College Dublin, Dublin 4, Ireland (e-mail: fault@fag.ucd.ie)*
[2]*Stratigraphy Group, Department of Earth Sciences, University of Liverpool, Liverpool, UK*
[3]*International Mining Consultants, PO Box 18, Mill Lane, Huthwaite, Sutton In Ashfield, Nottinghamshire NG17 2NS, UK*
[4]*Present address: Badley Earth Sciences, North Beck House, Hundleby, Spilsby, Lincolnshire PE23 5NB, UK*
[5]*Present address: Statoil ASA, D308, Forushagen, Grenseveien 21, N-4035 Stavenger, Norway*

ABSTRACT: The connectivity of reservoir bodies has been tested in unfaulted and variably faulted, high resolution 3D geocellular stratigraphic models (16 million cells in a 20 km × 20 km × *c.* 600 m volume) from the East Pennine Coalfield, UK. These deterministic stratigraphic–structural models are underpinned by high density borehole and mineplan data. The stratigraphy extends from mid-Westphalian A to base Westphalian C and represents a low net:gross (0.03–0.27) coal-bearing, delta top/fluvial reservoir analogue. The models contain up to 1467 post-depositional normal faults with maximum displacements ranging from 1 m to 140 m. Using two sets of facies as net, the effect of fault size on inferred reservoir connectivity has been assessed for stratal intervals with different sedimentary architecture, interval net:gross and thickness.

Faults often disconnect reservoirs in thinner, lower net:gross intervals containing only laterally discontinuous, channelized bodies. By contrast, faults generally increase reservoir connectivity in thick, relatively high net:gross intervals containing laterally extensive, tabular reservoir bodies. The most significant factor for fault-related reservoir connectivity is the dimensionality and scale of reservoir bodies in relation to the displacement distribution along faults. Populations of small, sub-seismic, faults (<5 m throw) can reconnect reservoir bodies that are dissected by larger displacement, seismic resolvable, faults (>20 m throw).

KEYWORDS: *fault (geology), reservoir model, reservoir characteristic*

INTRODUCTION

Fluid flow within faulted petroleum reservoirs is influenced by both fault-controlled juxtaposition of different flow units and the petrophysical properties of the fault rocks. Many studies have addressed the effects that fault rock content and permeability have on fault seal (e.g. Bouvier *et al.* 1989; Gibson 1994, 1998; Fulljames *et al.* 1997; Yielding *et al.* 1997) and flow (Lia *et al.* 1997; Manzocchi *et al.* 1999, 2002), but few have addressed the 3D geometrical aspects of faulting on reservoir connectivity. Fault juxtaposition effects are typically analysed using Allan diagrams (Allan 1989), sequence/throw juxtaposition diagrams (e.g. Bentley & Barry 1991; Knipe 1997) or aggregate connectivity plots (e.g. Childs *et al.* 1997), but these methods are strictly on a fault-by-fault basis. Here we focus on the 3D geometrical effects of a fault population and treat the faults as hydraulically neutral planes across which reservoir bodies can be connected or disconnected. This approach allows analysis of the geometrical effects that faults, and faults of different sizes, have on reservoir connectivity and is a useful prelude to studies that incorporate and examine the impact of fault petrophysical properties on flow.

The connectivity of faulted reservoirs is controlled by the interplay between a number of factors, which include the thickness and net:gross of the faulted interval, the size, dimensionality and distribution of reservoir units (e.g. King 1990), and the size and distribution of faults (e.g. Hesthammer & Fossen 2000). There is an inherent difficulty in determining the relative importance of these factors using traditional methods, mainly due to the uncertainties involved in determining the 3D sedimentary architecture and resolving the geometry and sizes of faults. The 3D distribution of reservoir bodies is commonly poorly constrained owing to seismic resolution and to sampling only by widely spaced wells. Similarly, the resolution of conventional seismic data limits the interpretation of faults to those with relatively large displacements (i.e. >20 m for most North Sea data; Badley *et al.* 1990; Walsh *et al.* 1994), thereby losing the detail of smaller faults that could have an impact on reservoir connectivity and flow (e.g. Sassi *et al.* 1992; Gauthier & Lake 1993; Omre *et al.* 1994; Walsh *et al.* 1998). To combat these limitations we have constructed a near deterministic, 3D faulted stratigraphic model derived from high quality, high density data from the Westphalian A–C succession of the East

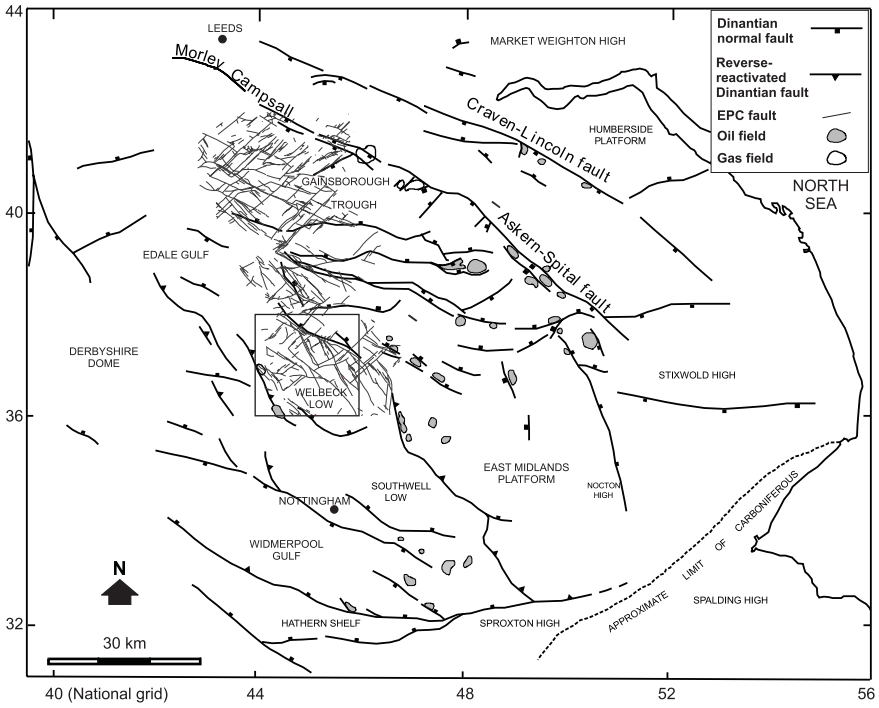

Fig. 1. Main structural elements and oil/gas field distribution in the East Midlands hydrocarbon province. Bold lines are reactivated, syn-rift Dinantian faults that underlie and offset the Coal Measures. Light lines show faults with maximum displacements >5 m in the East Pennine Coalfield. The location of the 20 × 20 km model area is shown. Regional scale map is redrawn from Fraser & Gawthorpe (1990).

Pennine Coalfield (EPC). The 3D geometry and distribution of stratigraphic elements is accurately constrained within a 20 km × 20 km × *c.* 600 m volume using a combination of 1100 boreholes, 64 wireline logs, mine plan and outcrop data. Within the same area, a database containing over two hundred 2 × 1 km coal extraction mine plans at a scale of 1:2500 has been used to produce a fault map that contains faults with maximum displacements down to 1 m. Three faulted stratigraphic models have been generated using three different resolutions of the fault population (throws >1 m, 5 m and 20 m). We have tested the difference in reservoir connectivity between the unfaulted and faulted models and use the results to demonstrate how (a) faults of different sizes, (b) the dimensionality of reservoir units, and (c) the interval net:gross, control the 3D connectivity of faulted reservoirs.

GEOLOGICAL CONTEXT

The 3D volume modelled measures 20 × 20 km × *c.* 600 m and is located in the southern part of the Westphalian EPC (Fig. 1). The Coalfield lies within the Pennine Basin, which was initiated during Dinantian rifting and superseded by thermal, post-rift sedimentation in the Namurian and Westphalian. The modelled stratigraphy extends from mid-Westphalian A to base Westphalian C (314–311 Ma; Fig. 2). The depositional environment was one of an easterly-flowing, fluvial delta top with the regional coastline located hundreds of kilometres to the east (Fraser & Gawthorpe 1990; Rippon 1997; O'Mara & Turner 1999). The stratigraphy is punctuated by regionally correlated 'marine bands', which record transient marine incursions into the prevalent freshwater environment (O'Mara & Turner 1999). The study area is also located within a region that has yielded a number of small oil (1–2 × 10^6 BBL recoverable) and gas accumulations sited within Dinantian, Namurian and lower Westphalian reservoirs, which have been exploited since the 1920s (Fig. 1; Fraser & Gawthorpe 1990).

The regional bed dips in the coalfield are typically gentle (*c.* 1–4° to the east), but are locally complicated by zones of folding, which either accommodate fault-related deformation or later Variscan folding (Goossens & Smith 1973). The fault

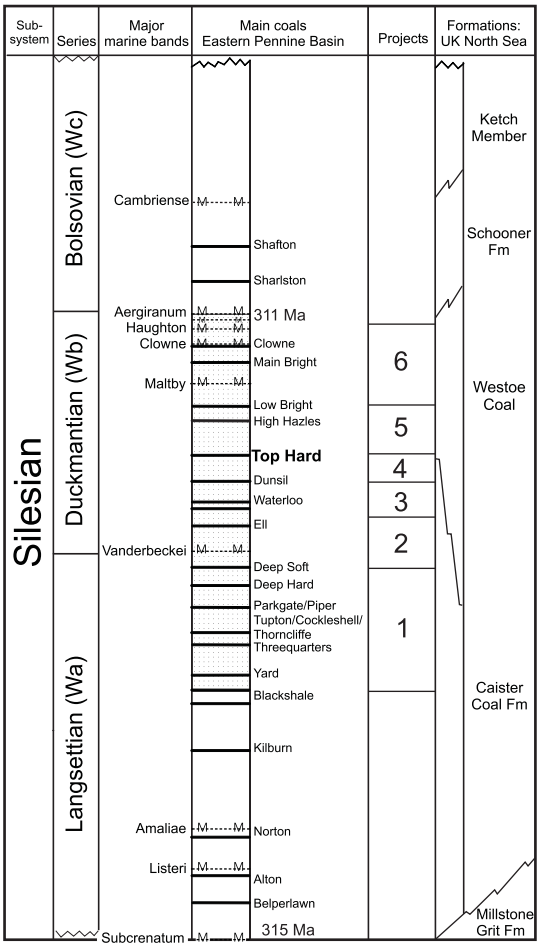

Fig. 2. Stratigraphy for the Westphalian A to C of the East Pennine Coalfield. The stratigraphic interval modelled is stippled. The limits of the separate stratigraphic intervals tested, referred to as 'Projects', are also shown. The Top Hard seam (bold) is used as the reference seam for the fault and structure contour 'pseudoseam' map.

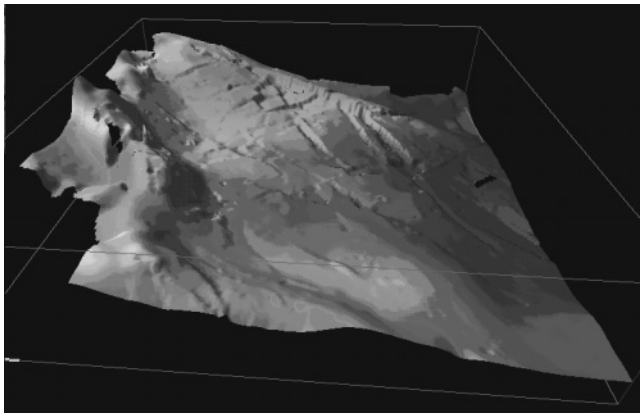

Fig. 3. 3D surface model for the 20 × 20 km Top Hard 'pseudo-seam'. View looking north. Faults are represented as vertical offsets of the surface. Regional dips are gentle and between 1° and 4° to the east, but locally complicated by NW–SE folds, such as the Brimington Anticline, located in the SW (left) of the area, which is interpreted as a Variscan inversion anticline. Structure contour values range from +400 m (light) down to −800 m (dark).

pattern is characterized by an orthogonal system of NE- and NW-striking faults, the majority of which are post-depositional, post-coalification normal faults with up to *c.* 200 m displacement (Rippon 1985*a*, *b*; Graham 1988; Walsh & Watterson 1988; Watterson *et al.* 1996). Some of the larger WNW–ESE-striking fault zones display evidence for a component of strike-slip displacement, but nevertheless preserve an overall normal sense of offset (Goossens & Smith 1973). Some of the NNW- to NW-striking faults have associated hanging wall folds, which are generally attributed to Variscan inversion (Fig. 1; Fraser & Gawthorpe 1990). One such structure, the Brimington Anticline (Fig. 3), occurs within the study area and is, on stratigraphical grounds, a mainly post-depositional Variscan structure. Occasional large throw (>100 m) syn-depositional faults also occur in the EPC (e.g. Morley–Campsall Fault; Fig. 1), but their syn-depositional displacements are pre-Westphalian and none are identified within the study area. Compactional or gravity-slide syn-depositional faults, which have a more limited vertical persistence (<50 m), are identifiable from mine plans and, apart from their localized association with certain seams, they are not significant within the model area and are excluded from our analysis. In summary, the vast majority of faults post-date lithification and display evidence of late Carboniferous to pre-Permian extensional displacements (Walsh & Watterson 1988).

MODEL CONSTRUCTION

The 20 × 20 km model area was chosen because of the high density and high quality of both sedimentological and fault data. The model building procedure, which is described in detail below, involved two main stages: (1) the construction of a stratigraphic model; (2) faulting the stratigraphic model using a structure contour map for a given coal seam. This procedure is appropriate for a volume in which the vast majority of faulting is post-depositional.

The stratigraphic model

The stratigraphy has been modelled using a database containing 1100 cored boreholes, 64 of which include wireline logs (gamma/density/caliper and some neutron and resistivity logs). Individual sedimentary bodies were modelled, in the main, by interpretation and correlation between boreholes (Rippon 2000). Additional constraints (e.g. facies correlation, sedimentary body geometries and internal lithological variations) were imposed using information from deep mines (e.g. mine plans, sedimentological plans at 1:10 000 or 1:2500, British Coal reports and records of sedimentological observations) and outcrop. The stratigraphy was separated into a series of intervals, bounded by time-stratigraphic markers such as regionally correlated coals and marine bands. Within each interval, the sedimentology was interpreted on a series of maps, containing isopach and facies distribution information, which were then digitized and imported into commercial 3D modelling software. Data from the maps were used directly to reproduce each sedimentary body and the high density of data (principally from boreholes) allowed good control on their geometries. Stochastic modelling of facies distributions and body geometries was not required at any stage of the modelling procedure and individual bodies in the model are treated as discrete objects. In all, 17 facies are identified in the modelled interval and potential reservoir units include multi-storey (<40 m thick and <15 km wide) and single-storey (2–15 m thick and tens to hundreds of metres wide) channels, overbank crevasse splay sheets (0.5–10 m thick) and rare mouth bars. Non reservoir units include well-drained floodplain siltstones, poorly-drained floodplain/lacustrine shales, marine/brackish water shales, coal seams (28 of which are regionally correlated time-stratigraphic markers) and palaeosols.

The full 3D sedimentological model was converted to a cellular format with cells defined by eight-corner point geometries. Cells are 200 × 200 m in plan view with variable thicknesses and each cell is assigned a discrete parameter (1–17), describing the facies. The result is a fully 3D, geocellular stratigraphic model that retains details of the facies distribution and the 3D geometry of each sedimentary body. The model varies from *c.* 500–650 m in thickness, comprising 407 layers and 16 280 000 cells. The upper *c.* 100 m of the model in the east is absent because the strata crop out.

The faulted models

There are insufficient data to produce a fully deterministic 3D fault model. Instead, a faulted 2D 'pseudoseam' map was constructed, and the 3D faulted model was built by extending the faults vertically. We refer to this map as a pseudoseam map because, although it is mainly based on one seam (the Top Hard), coverage on this seam is absent in certain areas in which case the structure has been extrapolated from seams up to 150 m beneath the Top Hard.

The Top Hard (Fig. 2) is by far the most extensively worked coal seam in the model area so it was used as the reference seam for the structural model. The map (Fig. 3) is based on British Coal seam abandonment mine plans from which fault traces, fault throws, fault tips, and seam elevation as spot points and contours were digitized. Localized compactional or gravity-slide syn-depositional faults are easily identifiable from mine plans and because these faults rarely extended from one coal seam to another, they were excluded from the model. The combination of data from different seams generates a small lateral shift of the fault traces of the same fault on adjacent seams. This effect arises from the dips of faults and is not significant on the scale of the study area. For further details of these data types and the map construction procedure see Watterson *et al.* (1996).

All of the available seam elevation data were gridded at 50 m spacing and refined using Zmap plus. Faults were incorporated during gridding as centre-lines and the seam surface was gridded up to faults providing discrete cut-offs. The final map

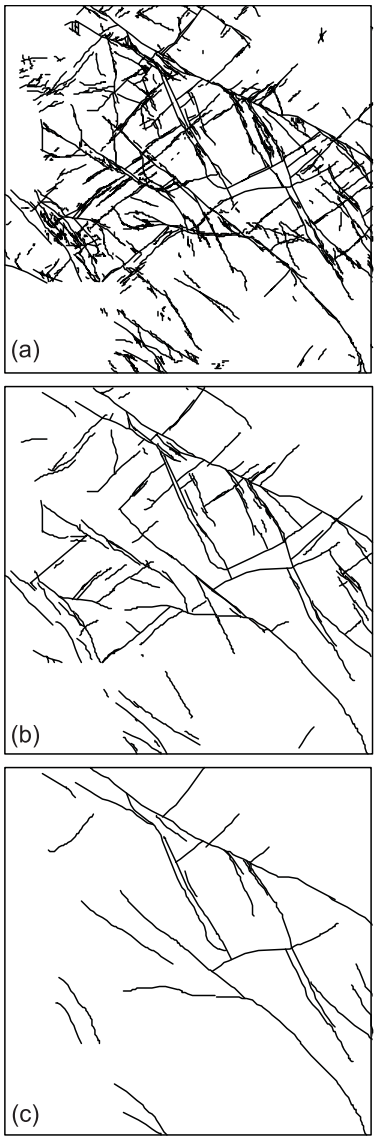

Fig. 4. Fault maps for the 20 × 20 km model area. Maps contain faults with maximum throws (a) >1 m (n=1467), (b) >5 m (n=154), and (c) >20 m (n=32), which are used to fault the 3D stratigraphic model.

contains all faults (n=1467) with maximum displacements >1 m and provides the highest resolution faulted model possible (Fig. 4a). The maximum displacement contained in the models is 140 m. Two lower resolution faulted models were also made; these contain faults with maximum displacements >5 m and >20 m (Figs 4b and c, respectively). The three models represent different resolutions of the same fault system with the 20 m fault map, for example, being equivalent to the resolution of a conventional (e.g. North Sea) seismic dataset, and the 5 m and 1 m models containing increasingly smaller, sub-resolution faults.

The three faulted pseudoseam models were processed to generate corner point data for a horizon. The corner point models are at 100 m resolution and faults that could be as far apart as 100 m are collapsed onto one fault, with the aggregated throw calculated. The final faulted cellular models were then generated by combining the corner point geometry for the Top Hard pseudoseam with isopachs of the stratigraphic succession. The end product of this process is a cellular model containing vertical faults, which preserve the fault geometry and the measured displacement variations along individual faults (Fig. 5). Although the faults have constant displacements in the vertical, our approach adequately reproduces the geometrical connectivity of the faulted succession for the purposes of this study.

ANALYSIS

The main aim of the study was to quantify the effects that faults of different sizes have on the connectivity of reservoirs. Tests were undertaken on the whole model volume (*c.* 500–650 m thick) and on six stratigraphic subdivisions (between *c.* 40 m and 200 m thick) with variable thicknesses, net:gross and sedimentary architectures. Each of the stratigraphic intervals is referred to as a '*Project*' with Project 1 being the lowermost (Fig. 2; Table 1). To further vary net:gross, two different sets of facies were used as net pay, namely: (1) only multi-storey and single-storey channel sandstones; and (2) all potential reservoir facies, including multi-storey and single-storey channel sandstones and siltstones, and both sandstone and siltstone overbank deposits. For descriptive purposes, a superscript suffix of 1 or 2 is used to describe which of the two different sets of facies are used as net, e.g. Project 1^1, refers to Project 1 with only clean sandstone-filled channels as net. The resulting Projects have variable, but relatively low net:gross (0.03 to 0.27). Testing of the resulting 52 models (4 faulted cases, 7 projects (total model and 6 intervals) and 2 sets of facies as net, but note that there is no Project 3^1; Table 1) provide a firm basis for comparing the quantitative systematics of reservoir connectivity, including and excluding faults. For convenience, faulted models for Projects containing faults with maximum displacements greater than 20 m are referred to as 20 m models, and similarly for those greater than 5 m and 1 m.

Analysis of reservoir connectivity in unfaulted and faulted models was undertaken by sampling the reservoir bodies using a regular, 2 km spaced array of 81 wells. The '*drainable volume*' functionality in Roxar's RMS v.6 was used to calculate the size and number of connected bodies and also the size of drainable volumes sampled by each well. Following Roxar's terminology, the volume of an individual body sampled by a well is referred to as a *connected volume*. A connected volume may be a sedimentologically isolated body or an interconnected body comprising a number of sedimentologically different systems that are juxtaposed by sedimentary processes or by faulting (Fig. 6). A *drainable volume* is used to describe the total volume of reservoir bodies sampled by a well and may, therefore, comprise one or more connected volume(s). In this type of analysis, the faults are treated as hydraulically neutral planes across which reservoir bodies can be dissected or juxtaposed against other bodies.

For each model, tests have been undertaken using the whole 81 well array and smaller arrays comprising 4 (2 × 2), 16 (4 × 4) and 64 (8 × 8) wells. These arrays were positioned systematically around the model resulting in 64 arrays of 4 wells, 16 arrays of 16 wells and 4 arrays of 64 wells. The aim of this well sub-sampling procedure was to test the variability, or risk, associated with implementing different well strategies to sample variable faulted sedimentological architectures.

RESULTS

Changes in reservoir connectivity between the unfaulted and faulted models can be illustrated by reference to two end-member cases, in which faults either increase (e.g. Project 1^2) or decrease bulk connectivity (e.g. Project 2^1). Projects 1^2 and 2^1 are also sedimentological end-members; Project 1^2 is the highest net:gross (0.27) interval tested and contains extensive

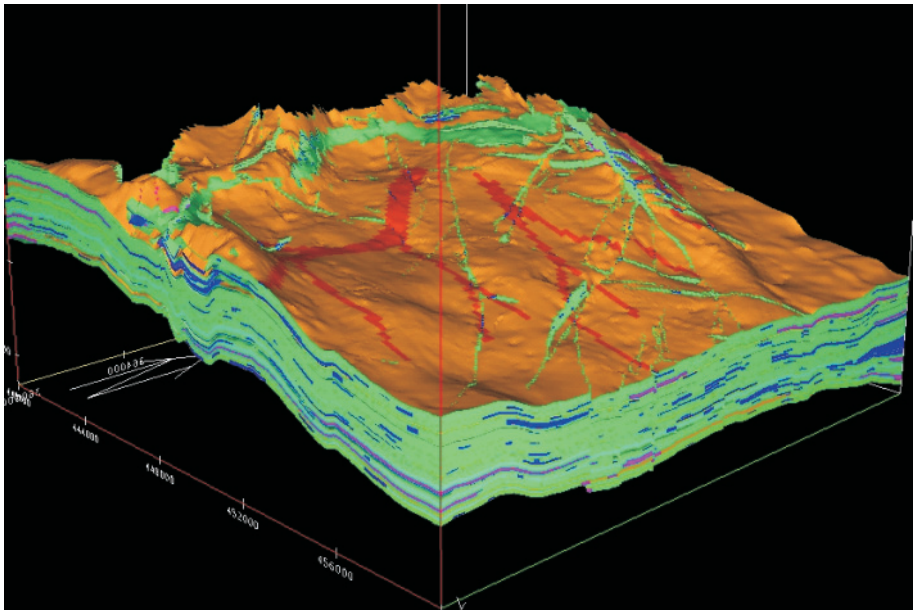

Fig. 5. Complete 3D geocellular, faulted stratigraphic model. The model is 20 km × 20 km × *c.* 600 m. 17 facies are identified and are colour coded (e.g. mudstone and siltstones are green, sandstone- and siltstone-filled channels are pink and dark blue, respectively). × 5 vertical exaggeration and view looking northwest. Note the offset of layers along vertical faults.

tabular bodies (Fig. 7a), whilst Project 2^1 is the lowest net:gross (0.03) and contains only disparate channels (Fig. 7b). We also present the analytical results for Projects 2^2 and 6^1 (Figs 7c and d, respectively), which are not end-member cases and, like most of the models tested, display hybrid characteristics.

High net:gross, thick successions (Project 1^2)

Figure 7a shows the 3D geometry of all potential reservoir units in Project 1^2. This is the lowermost, thickest (*c.* 140 m thick) and highest net:gross (0.27) Project in the model. The main facies types display different sedimentological geometries, ranging from interconnected multi- and single-storey channel systems to areally extensive, tabular overbank deposits. The channel systems are distributed throughout the interval and two overbank deposits are located within the central to lower parts. These unfaulted geometries mainly define *laterally* well connected systems, but they are poorly connected *vertically* and therefore in 3D, because of the near 2D nature of the sedimentary units and their vertical separation across coal, shale and mudstone layers and packages.

An illustration of the results obtained from connected and drainable volume tests is presented in Figure 8, which shows that there are more bodies in the unfaulted model and there is a much larger largest body in the 1 m faulted model.

Table 1. *Details of all models/Projects tested*

Model/Project	No. layers	Net^1	Net^2	$D_A{}^1$	$D_A{}^2$
All	407	0.05	0.17	0.964	0961
6	67	0.04	0.13	0.979	0919
5	52	0.05	0.14	—	0.938
4	28	0.06	0.17	—	0.941
3	56	—	0.11	—	0.933
2	58	0.03	0.09	0.917	0.982
1	146	0.1	0.27	0.967	0.977

Grey shading shows the Projects presented in the main text. Project 3 contains no clean reservoir facies. D_A refers to the area weighted dimensionality of reservoir bodies within each Project (see text for discussion). Net^1, clean reservoir facies, including only multi- and single-storey sandstones; Net^2, all potential reservoir facies, including multi- and single-storey sandstones and siltstones, and overbank siltstones and sandstones.

Qualitatively, this observation suggests that the faulted model is better connected than the unfaulted. The plots in Figure 9 are used to quantify the differences in connectivity between the unfaulted and faulted models. Figure 9c shows that most of the

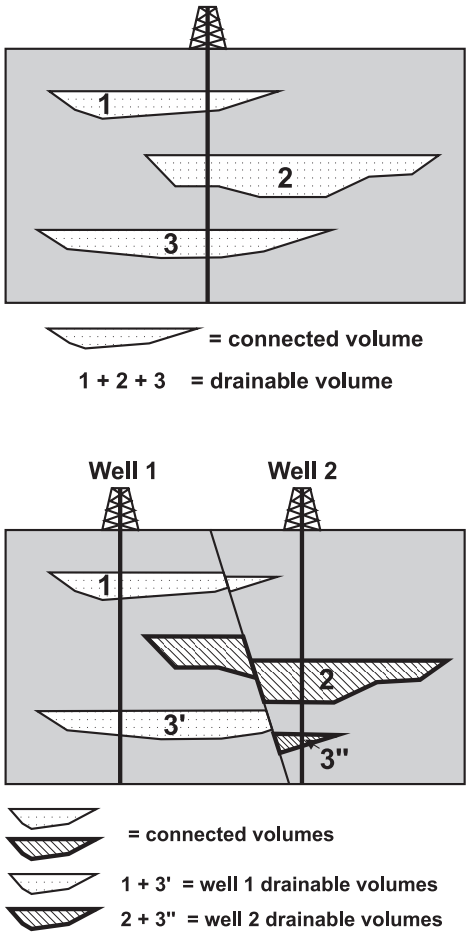

Fig. 6. Details and terminology involved in well tests. A *drainable volume* is the sum volume of a series of spatially isolated reservoir bodies, referred to as *connected bodies* or *volumes*, sampled by a well or well array.

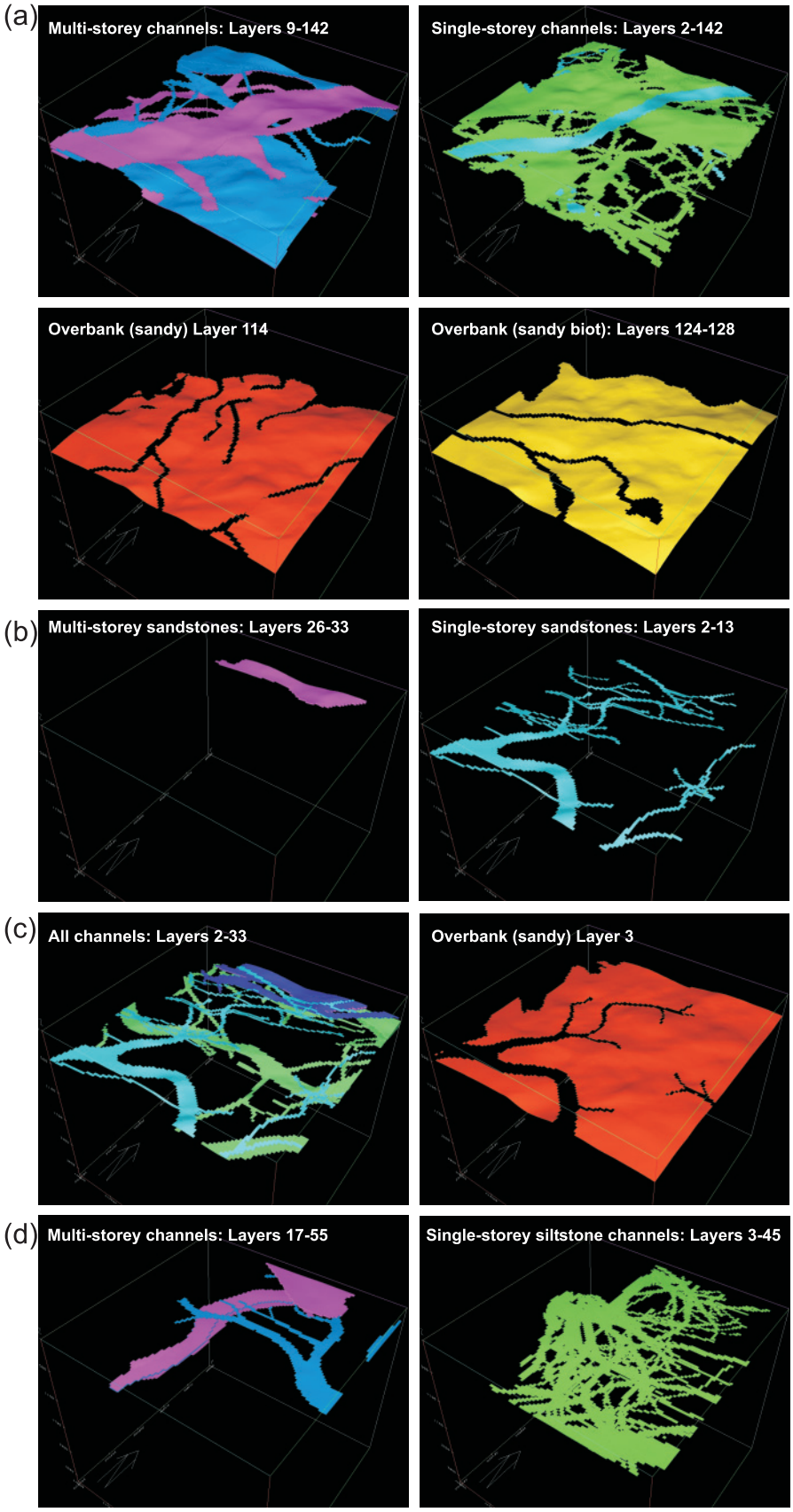

Fig. 7. Reservoir bodies within (**a**) Project 1^2, (**b**) Project 2^1, (**c**) Project 2^2 and (**d**) Project 6^2 for the 20 × 20 km model area. These Projects are described in the text and their connectivity test results are presented in Figures 8 to 13. Views are to the northwest and units are colour coded for facies type: pink, multi-storey sandstone channels; blue, multi-storey siltstone channels; light blue, single-storey sandstone channels; green, single-storey siltstone channels; orange, sandstone overbank deposits; yellow, bioturbated sandstone overbank deposits.

27 reservoir bodies in the unfaulted model are juxtaposed across faults to create a much larger largest body in the faulted models (3.7 km^3 as opposed to 15 km^3; Fig. 9c). The reduction in curve gradient from the unfaulted to progressively more faulted models in this plot indicates that progressively more bodies are juxtaposed to create a larger largest body. This largest body in the faulted models is large enough to be sampled by all 81 wells, which results in the much more

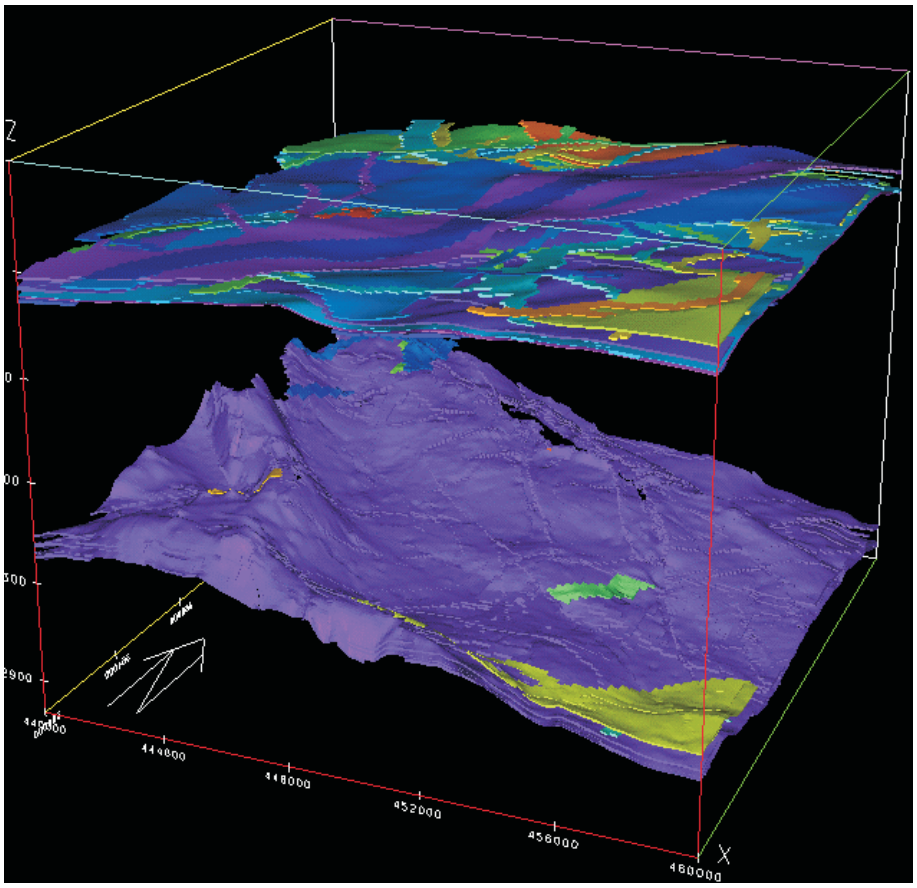

Fig. 8. 3D visualization of the 20 × 20 km model area illustrating the size and distribution of connected volumes (individual reservoir bodies) in Project 1[2] sampled by the 2 km spaced, 81 well array in the unfaulted (top) and 1 m faulted (bottom) models. Each connected body is colour coded and shows that the 1 m model is dominated by one very large connected body (purple), whilst the unfaulted stratigraphy contains numerous (28) bodies. The unfaulted model is poorly connected vertically but, with the addition of 1 m maximum throw faults, vertically disposed reservoir units are juxtaposed to create a well connected system.

homogeneous distribution of drainable volumes than the unfaulted model (i.e. compare Fig. 9a with b; Fig. 9d). The size of possible drainable volumes sampled by each well is highly variable in the unfaulted model (2.5 to 10.4 km^3; Fig. 9d), but near constant in the faulted models (e.g. 15.4 to 15.6 km^3 for the 5 m and 1 m models; Fig. 9d).

In detail, the addition of the 20 m maximum throw fault population results in a drastic increase in connectivity and drainability relative to the unfaulted model (Figs 9c, d and e). This is because the largest faults in the area are responsible for juxtaposing most of the reservoir units to create a very large, largest body (14 km^3; Figs 9c and 9d) that is sampled by all 81 wells. The effect of adding the 5 m and 1 m faults is to juxtapose additional smaller bodies against the largest body to increase its size (15.3 and 15.4 km^3, respectively; Figs 9c and 9d). Therefore, with the progressive addition of more smaller faults (20 m, 5 m and finally 1 m) there is a progressive increase in the size of the largest body and a decrease in the number of bodies (Fig. 9c). This results in a progressive decrease in variability in the size of drainable volumes sampled, which is particularly evident at low well densities (Figs 9e and 9f). However, it is the largest faults in the area that have the most significant impact.

The variability associated with drilling the unfaulted and faulted models using different well densities is shown in Figure 9f. The advantage of this type of plot is that it shows the potential risk associated with implementing different well strategies. The curves for the faulted model show substantially less variability (i.e. curve gradients are steep) and they are always shifted to the right of the equivalent curve for the unfaulted model because the faulted models are significantly better connected. This difference is most distinct for low well densities (i.e. 1 or 4 wells) because there is a substantially lower probability of hitting a sizeable drainable volume in the unfaulted model than in the faulted models. For example, using one well, the size of potential drainable volumes ranges from 2.5 to 10.4 km^3 in the unfaulted model, whereas larger and more similar sized volumes (15.4 to 15.6 km^3) are sampled in the faulted model. However, when progressively more wells are used in the arrays the variability associated with drilling the unfaulted sedimentology decreases (the curve gradients steepen) and the size of the drainable volumes increases (the curves shift to the right).

These results clearly demonstrate that inclusion of the geometric effects of faulting significantly increases reservoir connectivity in this model.

Low net:gross, thin successions (Project 2[1])

Figure 7b shows the 3D geometry of clean reservoir facies in Project 2[1], which directly overlies Project 1 and is a thin (58 layers and *c.* 75 m thick), low net:gross (0.03) succession. This interval is dominated by two main sedimentary systems, namely a channelized single-storey system in the south and a multi-storey body in the north. The unfaulted sedimentology is poorly connected laterally and vertically because of the small number and wide distribution of reservoir units. The effect of faulting is to further dissect the system and, more specifically, there is a progressive dissection of the channel systems with an increase in the number of faults (Fig. 10).

Figure 11 shows the equivalent plots to Figure 9c to 9f for Project 2[1]. The plots show that although the largest body in this Project (the northern multi-storey body) remains intact in all faulted models, the second largest body is disconnected by faulting and further disconnected with the addition of 5 m and 1 m maximum throw faults (Figs 10 and 11). Figures 11 c and

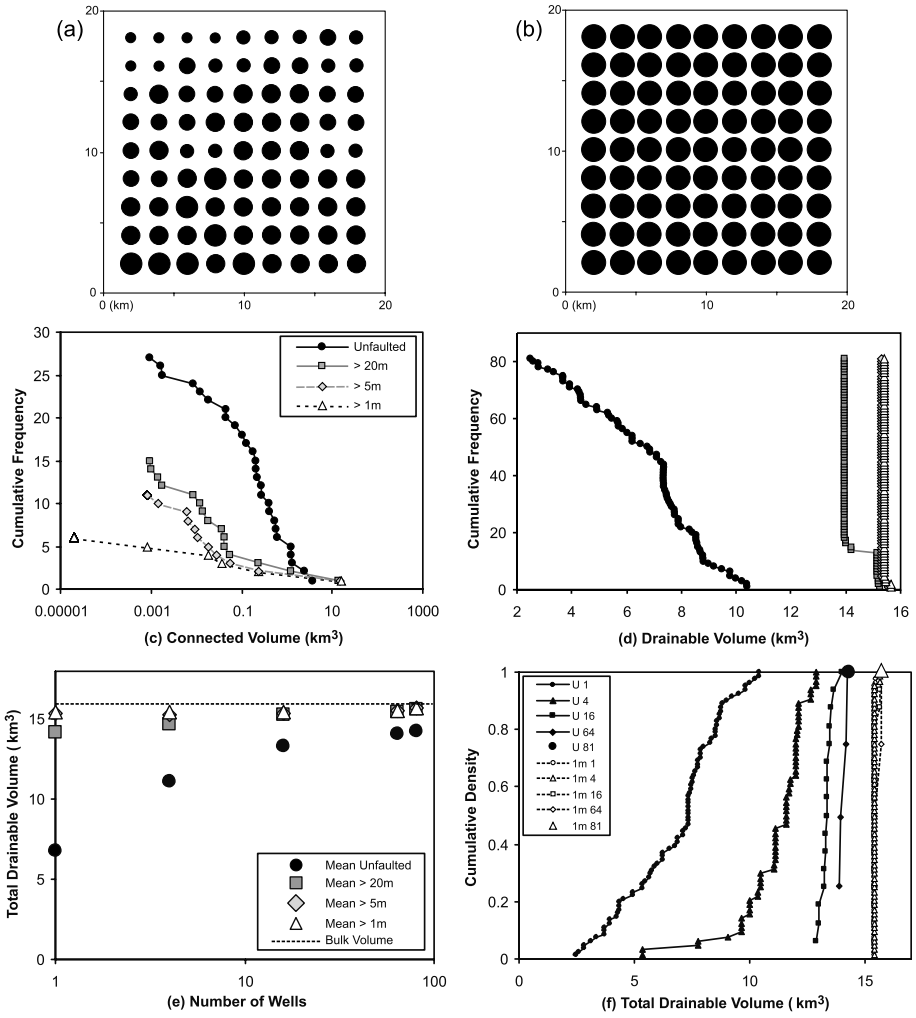

Fig. 9. Plots showing the difference in the size and number of connected and drainable volumes between the unfaulted and variably faulted models in Project 1^2. (**a**) and (**b**) Map view 'bubble plots' of the 20 × 20 km model area showing the relative size of drainable volumes sampled by each of the 81 wells in the (a) unfaulted and (b) 1 m faulted model. The size of the bubble is proportional to the size of the drainable volume sampled. (**c**) Cumulative frequency plot showing the size distribution of connected volumes (individual bodies) sampled by the 81 well array for the 4 fault cases. (**d**) Cumulative frequency plot of the drainable volumes sampled by each of the 81 wells for all fault cases. (**e**) Variability in the mean drainable volumes in the unfaulted and all faulted models sampled by different sized well arrays (from left to right, individual wells and arrays of 4, 16, 64 and 81 wells). (**f**) Total drainable volume distributions plotted as a function of well density (i.e. the number of times the well arrays are used to sample the 81 wells) for the unfaulted and 1 m faulted models. See text for discussion.

d demonstrate that there is substantial risk and variability associated with drilling *both* the unfaulted and faulted sedimentology using all well arrays. For example, there is a high probability of missing reservoir units using ≤ 4 wells in an array (Fig. 11d). Even when more than 4 wells are used to sample both unfaulted and faulted models, the range of potential drainable volumes is *c.* 0.1 to 0.8 km^3. However, what is most significant is that in Figure 11d the curves for the faulted model provide lower drainable volumes than the equivalent curve for the unfaulted model because the faulted model is less connected.

Faulting in this case results in a progressive reduction in connected and drainable volumes, which is due to the efficient manner in which faults offset successions comprising mainly channelized, i.e. essentially 1D, reservoir bodies. In all models, however, the northern multi-storey body remains intact and is the largest body throughout.

Inclusion of tabular reservoir bodies (Project 2^2)

Project 2 was also tested using all potential reservoir facies as net pay, which has the effect of including some minor siltstone-filled channels and, most significantly, one large overbank deposit (Fig. 7c). The resultant suite of plots (Fig. 12) is equivalent and directly comparable to those in Figure 11. Figure 12a shows that with the addition of large (20 m) faults to the unfaulted model the size of the largest connected body increases significantly and also the gradient of the curves progressively shallow from the unfaulted to 20 m to 5 m to 1 m models. These two effects, as with Project 1^2 (compare with Fig. 9c), are indicative of faults, and the progressive addition of smaller faults, increasing connectivity and the size of drainable volumes sampled (Figs 12b, c, d). Figures 12c and 12d show that no matter what well strategy we use, the faulted models, and in particular the most faulted models, are better connected than the unfaulted model.

The reason for the distinct change in the response to faulting from Project 2^1 to Project 2^2 is the addition of an overbank deposit which, because it is laterally extensive, has a high probability of being juxtaposed against vertically disposed channels across faults. The addition of just one reservoir body to Project 2^1 is therefore responsible for a change from a system where faults disconnect reservoir units (Fig. 11) to one in which faults increase connectivity (Fig. 12).

Hybrid effects (Project 6^2)

Project 6^2 is a relatively thick (67 layers; 75 to 150 m thick), intermediate net:gross (0.13) interval that contains laterally well connected channel systems (Fig. 7d). With the addition of the larger 20 m and 5 m faults to the unfaulted model the size of the largest connected body decreases (inset, Fig. 13a). However, the effect of the >1 m maximum throw population is to reconnect the system to create a significantly larger largest body than the other unfaulted or faulted models. This effect, as seen for Projects 1^2 and 2^2, results in the 1 m model being more

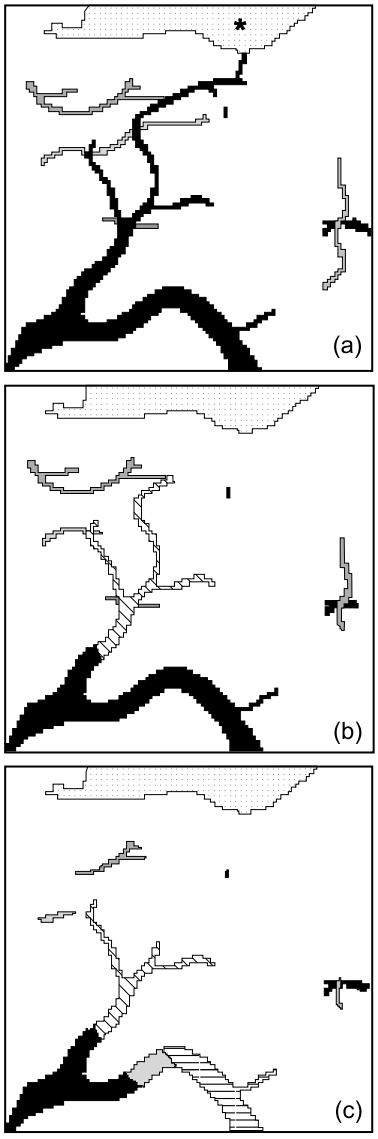

Fig. 10. Maps showing reservoir connectivity for the 20 × 20 km model area for (**a**) unfaulted, (**b**) 20 m faulted and (**c**) 1 m faulted models in Project 2[1] sampled by the 81 well array. Separate connected bodies are highlighted by different ornament. (**a**) The unfaulted system is dominated by a thick multi-storey channel body in the north (*) and a relatively well connected single-storey channel system (black; also see Fig. 7b). (**b**) With the addition of 20 m maximum throw faults, the single-storey channel system and subsidiary channels are offset. (**c**) With the incorporation of 1 m faults, the channel systems are further dissected.

'drainable', which is evident from Figures 13b and 13c. However, the unfaulted, 20 m and 5 m models display 'hybrid' curves in that the unfaulted model possesses the largest body and the 5 m the smallest (inset, Fig. 13a), whilst, on average, the curve in the 5 m model is shifted to the left of the unfaulted. This contrasts with the previous models in that the model with the largest connected body also produced the shallowest curve gradients. This complexity is also observed in Figure 13b, in which the unfaulted model yields by far the largest drainable volume (2.2 km^3) but, on average, the 20 m and 5 m models produce larger drainable volumes of intermediate size (i.e. between 1 and 1.5 km^3). In contrast, the 1 m model yields consistently larger drainable volumes.

The complexity displayed above by the various models is compounded in Figure 13c, in which the 1 m model yields the

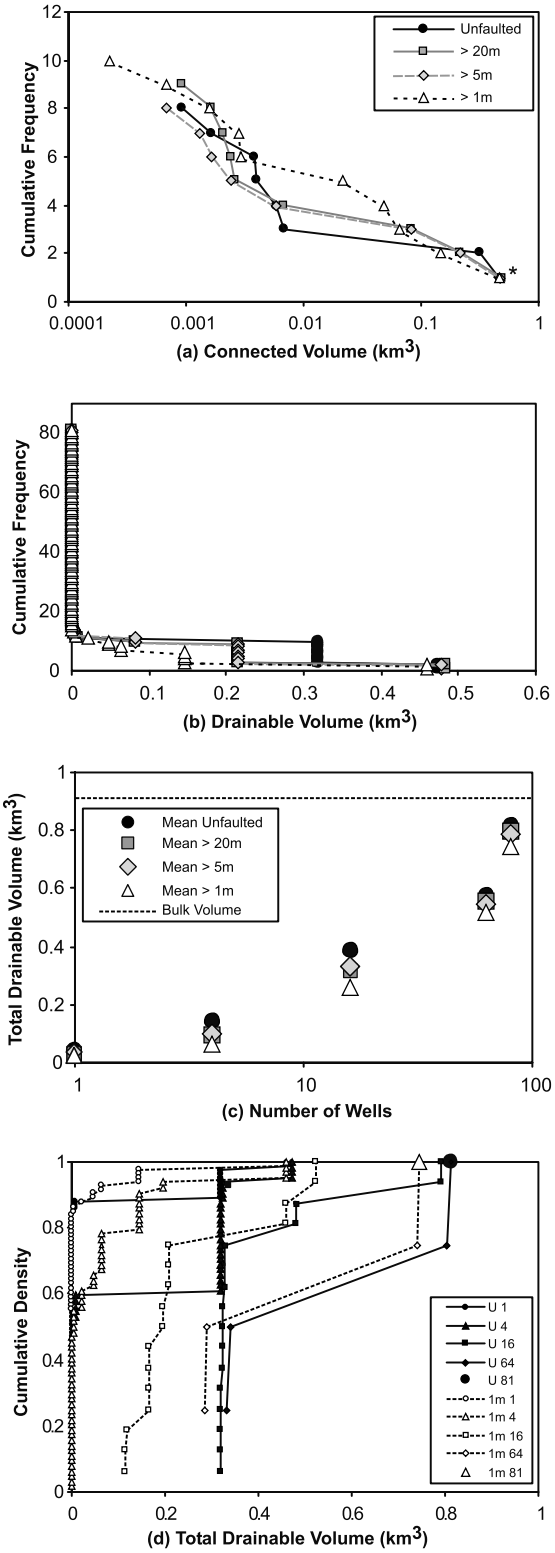

Fig. 11. Results of connected and drainable volume tests in Project 2[1], which are equivalent to the plots shown in Figures 9c–e. (**a**) and (**b**) Cumulative frequency distributions of (a) connected and (b) drainable volumes showing a progressive decrease in connectivity from the unfaulted to progressively more faulted models. * in (a) shows the position of the multi-storey body. (**c**) Mean drainable volumes sampled using the various well arrays. The incorporation of progressively smaller faults results in a progressive decrease in the size of the mean drainable volume sampled. (**d**) Drainable volume size distributions as a function of well density showing that, regardless of the well array used, the volumes sampled are highly variable for both the unfaulted and 1 m faulted models.

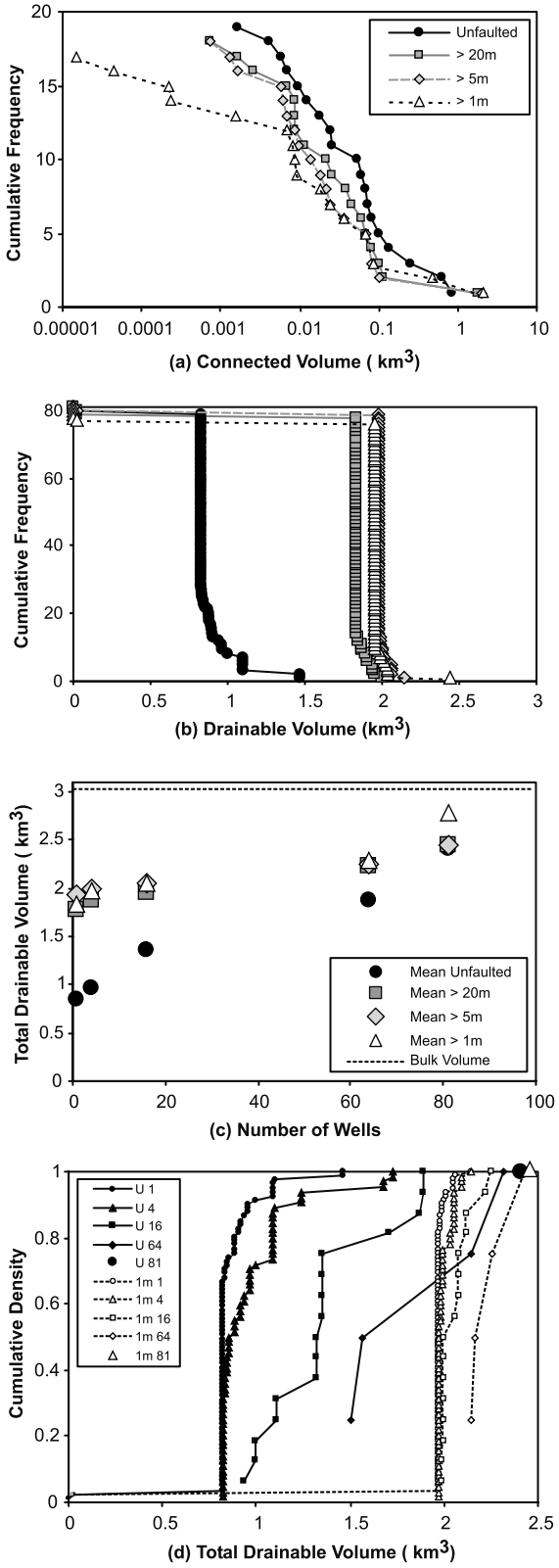

Fig. 12. Details of connected and drainable volume tests for Project 2^2. Cumulative frequency distributions of (**a**) connected and (**b**) drainable volumes showing that there is a progressive increase in connectivity as a function of adding progressively smaller faults. (**c**) Mean total drainable volumes show that the faulted models are better connected, particularly at low well densities and, in general, that the 1 m model is the best connected. (**d**) Drainable volume size distributions as a function of well density showing that the 1 m model is consistently better sampled than the unfaulted model.

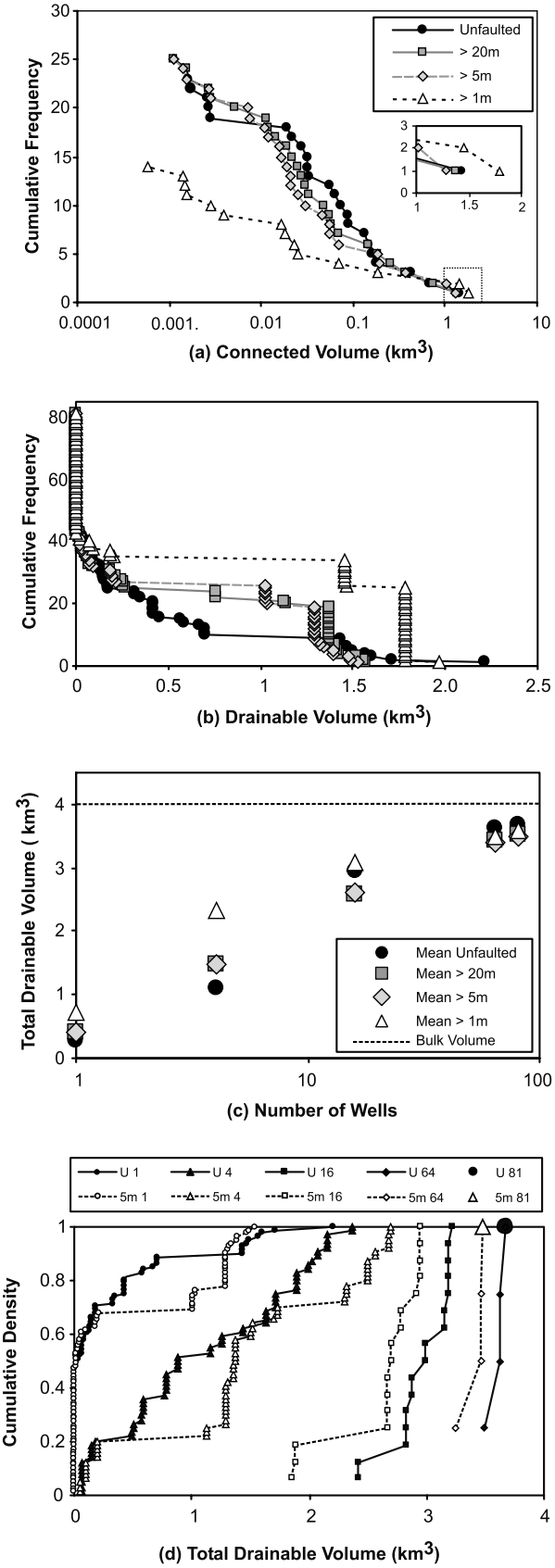

Fig. 13. Details of connected and drainable volume tests for Project 6^2. Cumulative frequency distributions of (**a**) connected and (**b**) drainable volumes. (**c**) Mean drainable volumes sampled by the different well arrays. (**d**) Drainable volume size distributions as a function of well density for the unfaulted and 5 m models. See text for detailed description and discussion of plots.

largest mean drainable volumes and the unfaulted the smallest when sampled by low well densities ($\leq$16 wells), but at high densities the unfaulted model is the best sampled. The dependence of drainable volumes sampled on the size of the well array used helps to explain the cause of the complexity in this Project, which characterizes most of the Projects tested. The addition of the largest faults (i.e. those with maximum displacements >5 m) to the unfaulted model causes various parts of the channel systems, including the largest unfaulted body, to be disconnected, thereby reducing the total potential reservoir volume. However, the same faults also connect other channels to generate, on average, larger connected bodies and a more homogeneous distribution of 'intermediate' sized volumes. Therefore, at high well densities there is more potential volume to be sampled in the unfaulted model, but at low well densities there is a higher probability of the wells sampling one or more sizeable volumes in the faulted model. By comparing the unfaulted model with the 5 m, Figure 13d highlights this 'switch' from a situation where low well densities ($\leq$4 wells) sample the 5 m model more efficiently to one in which the unfaulted model is better sampled at higher well densities ($\geqq$16 wells).

In this example, the effect of the 1 m maximum throw population is the most significant. Faults with displacements between 1–5 m reconnect parts of the system that were disconnected by the larger faults, which results in the 1 m model possessing the largest connected volumes. As a consequence, the 1 m model yields consistently large drainable volumes (Figs 13a, b and c).

SENSITIVITY OF TEST RESULTS TO THE DIMENSIONALITY OF RESERVOIR UNITS

A summary of test results for all unfaulted, 1 m and 20 m models is shown in Figure 14, which highlights the change in the % net sampled by the 81 well array as a function of net:gross and with the addition of faults. In general, the higher net:gross models (*c.* >6%) are better connected by the addition of progressively smaller faults. Lower net:gross models (*c.* <6%), on the other hand, are usually disconnected by faults. Although these results would suggest that net:gross is the overriding control on the connectivity of faulted reservoir units, the absence of a strong correlation indicates that there are additional controls. Significantly, the only Projects that show an increase in drainability from both unfaulted to 20 m faulted models and from 20 m to 1 m faulted models are those containing laterally extensive, sheet overbank deposits (* in Fig. 14). Therefore, the presence of extensive tabular bodies, even within low net:gross successions, has the effect of connecting vertically and laterally separated reservoir bodies within faulted models (e.g. Project 2^2; Fig. 12). The broad equivalence between net:gross and connectivity is however consistent with the weak association between high net:gross successions and the presence of laterally extensive reservoir bodies.

In an attempt to quantify the impact of the size and geometry of reservoir bodies on faulted connectivity, we use a number of quantitative geometric attributes of reservoir bodies. Each body is assigned a size, which is taken as the areal dimensions of the body. The *dimensionality* of a body is defined by the expression

$$D = N/N_m$$

where D is the 'areal dimensionality', N is the number of cell face-to-cell face connections and N_m is the maximum possible number of cell face-to-cell face connections. For example, a

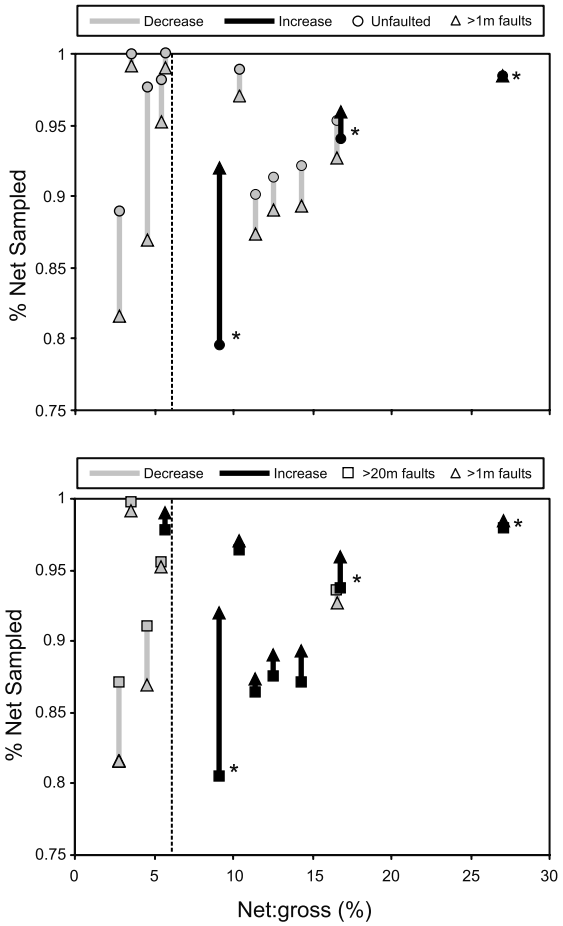

Fig. 14. Comparison of the change in connectivity with the addition of all faults to (**a**) unfaulted strata and (**b**) >20 m fault cases in various Projects. Grey lines show those models that are less connected with the addition of faults (a) and progressively less connected with the addition of more smaller faults (b); these models are typically low net:gross (<6%, dotted line). Black lines show those models that are better connected with the incorporation of faults and with the addition of more smaller faults.

perfectly linear body comprising 36 cells with a uniform width of 1 cell has a total of 70 cell face-to-cell face connections (i.e. it is a 1D body). The maximum number of possible connections (N_m) for 36 cells is 120, assuming they are arranged as a square (i.e. a 2D body). Therefore, for the 1D body D=0.56, whilst D=1 for the 2D body. D is also dependent on the number of cells, but this effect is small for the bodies in this model which typically contain more than 50 cells. A D value of 1 could describe a small (2 × 2 cells) or large (200 × 200 cells) body, though their effects on connectivity are completely different. It is necessary therefore to consider D and size together. Figure 15a shows D plotted against size (plan view area) for each of the reservoir bodies in the whole 3D model. Although there is a positive correlation there is greater than one order of magnitude variation in size for a given D. This broad positive correlation demonstrates that the largest bodies in the model tend to have higher dimensionality on the scale of the study area, i.e. they form sheets, wide channels or branching systems. In contrast, the smaller bodies in the model tend to be narrow, single channels. The hypothesis to test is whether or not intervals dominated by bodies that plot in the upper right of Figure 15a are better connected by faulting than intervals containing only smaller channelized bodies that plot towards the lower left. In order to describe an average size and

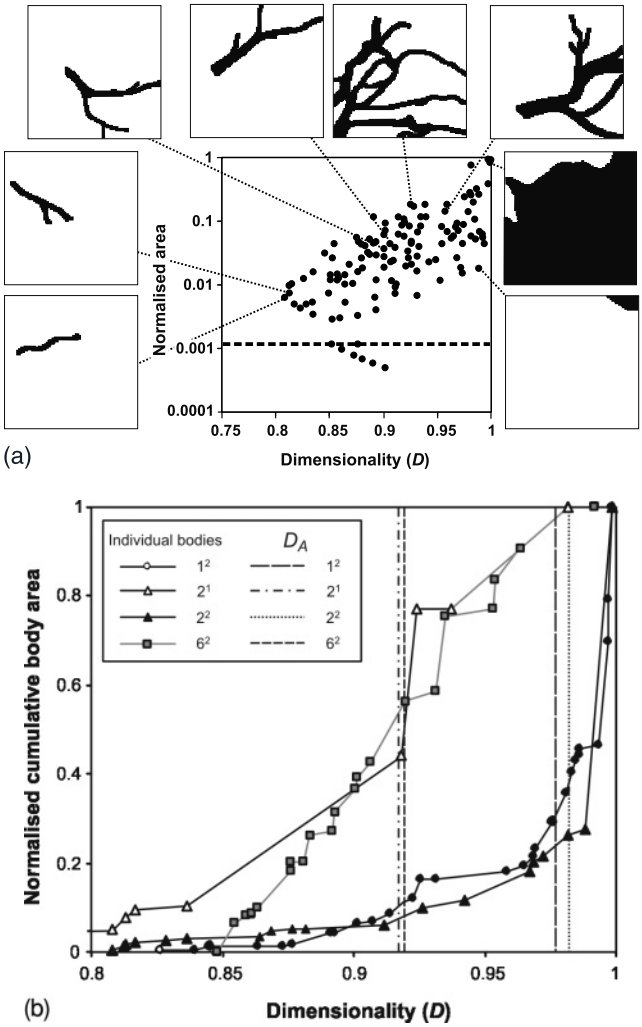

Fig. 15. Details of the size and dimensionality of reservoir bodies in the model with example reservoir bodies (black) shown in plan view (20 × 20 km squares). (**a**) Dimensionality (D) of connected bodies in the unfaulted model plotted against their plan view area (normalized to the model size). Bodies that lie below the dashed horizontal line, which correspond to bodies comprising 50 cells (500 000 m^2 in area), are not completely represented in the model and are considered insignificant in terms of system connectivity. (**b**) Normalized cumulative distribution of the dimensionality of reservoir bodies in Projects 1^2, 2^1, 2^2 and 6^2. Vertical lines show the area-weighted dimensionality (D_A) of reservoir bodies for each Project. See text for discussion.

dimensionality of reservoir bodies within a Project, we use area weighted dimensionality (D_A: Table 1):

$$D_A = \Sigma DA/\Sigma A$$

where A is the plan view area of the body. This attribute gives higher weighting to those bodies with larger areas because they are the most important in terms of contributing to the gross connected volumes. D_A values for the four Projects discussed in the previous section are plotted in Figure 15b along with the corresponding curves for reservoir body D. The reservoir bodies from which these curves are derived are shown in Figure 7. The curves in Figure 15b for Projects 2^1 and 6^2 display nearly constant gradients, defined by reservoir bodies of comparable size and dimensionality, which yield relatively low D_A values. In contrast, the curves for Projects 1^2 and 2^2 exhibit steep right-hand segments, defined by laterally extensive overbank deposits, which dominate the distribution and produce high D_A values: Projects with these characteristics are expected to be better connected by faulting than those with nearly straight curves and low D_A, as we have demonstrated in the previous examples.

Although net:gross is an indirect determinant on whether or not a system is better connected by faulting, the dimensionality of the unfaulted strata is critical. Channelized bodies, which approximate 1D (i.e. linear) elements, have a high probability of being disconnected by faults. Conversely, laterally extensive, tabular bodies, which approximate 2D (i.e. planar) elements, have a high probability of being juxtaposed against vertically separated units across faults. This juxtaposition effect is very efficient, because individual faults have laterally varying displacements and can therefore juxtapose numerous units along their length, a feature which is returned to in the next section. Quantitative links can be defined between the effects of faults and the dimensionality of faulted units. Figure 16 shows the average dimensionality (D_A) of reservoir units within a Project plotted against the % reservoir volume sampled by different well arrays; Projects 3^1, 4^1, 5^1 and 6^1 are not included because they either contain no clean reservoir sand facies or they contain only one or two reservoir bodies. The positive correlation between D_A and % reservoir volume sampled demonstrates that intervals containing larger, more tabular bodies are generally better connected before faulting, and even better after faulting. Furthermore, a characteristic of all but one of the Projects is that 1 m faulted models are generally better connected than the unfaulted or other faulted models, a feature which is discussed in the next section.

SENSITIVITY OF TEST RESULTS TO THE SCALING OF FAULTS AND RESERVOIR BODIES

Our analysis shows that for the relatively low net:gross (0.03–0.27) successions of the EPC, the dimensionality of the unfaulted strata is a determining factor on whether faults increase or decrease the connectivity of reservoir units. The reasons for this can be explored further, by considering the relative scales of faults and of sedimentary bodies. All faults show displacement variations along their length and can, ideally, be characterized by a maximum displacement and a length. Similarly, the dimensions of sedimentary bodies, such as channels, can be described in terms of their maximum thickness and width. A fault cannot entirely offset a sedimentary body if its maximum displacement is less than the thickness of the sedimentary body. Even for a fault which has a maximum displacement greater than the thickness of a sedimentary body, complete offset of the body will only occur if the local displacement along the faulted body is greater than the local body thickness. This factor is controlled not only by the relative locations of intersecting faults and bodies but also by their displacement:length and the width:thickness ratios. When the fault maximum displacement and the reservoir body thickness are the same, disconnection is more likely to be achieved when the fault maximum displacement:length ratio is lower than the channel width:thickness ratio (i.e. the fault is laterally more persistent), whereas juxtaposition is optimized if the displacement:length ratio is higher than the width:thickness ratio (i.e. the channel is laterally more persistent). The likely impact of different factors can be explored by comparing the dimensions of all faults and reservoir bodies in the model (Fig. 17). For 20 m fault models not containing tabular overbank facies, the faults are generally larger than reservoir bodies and are therefore responsible for a decrease in connectivity. For 1 m fault

models, by contrast, the majority of faults in the EPC model have displacements less than the thinnest channels (*c.* 5 m), resulting in an increase in connectivity. The inclusion of overbank facies which, despite their relatively low thicknesses, are laterally more persistent than any of the faults, has the effect of increasing the connectivity of models: although the overbanks are often entirely offset by individual faults their lateral persistence permits connectivity to be preserved beyond the ends, i.e. tips, of individual faults.

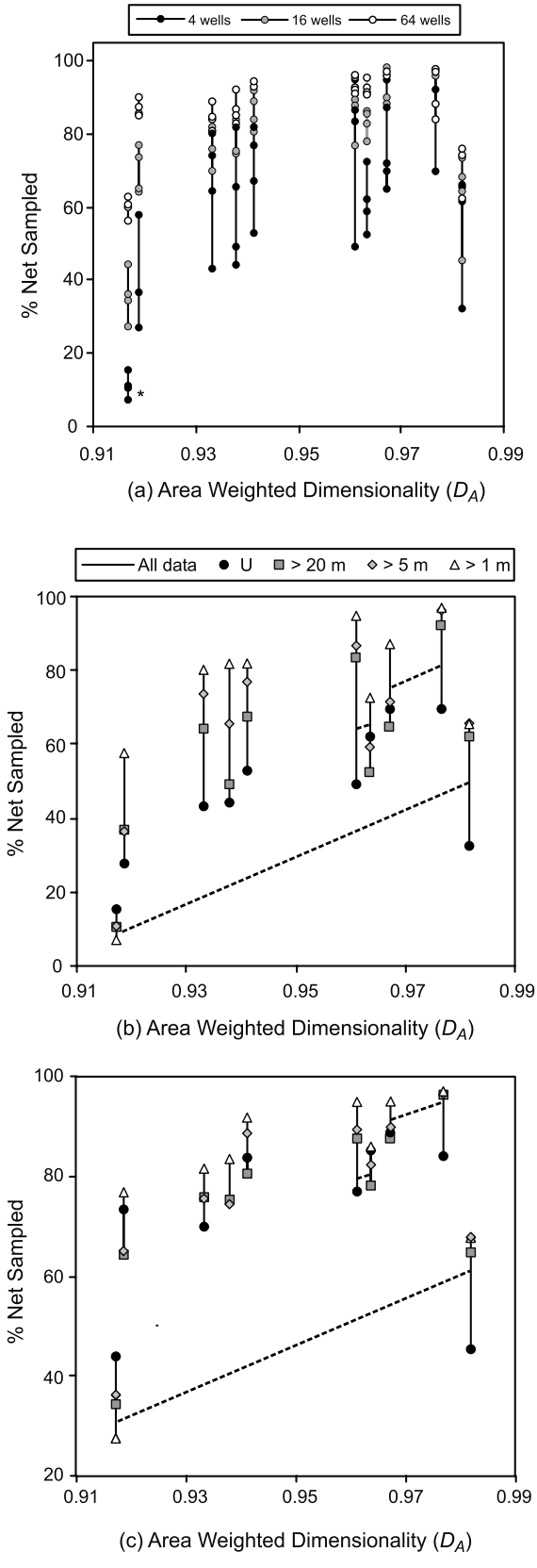

Fig. 16. Area weighted dimensionality (D_A) for each Project plotted against % reservoir sampled by the various well arrays. (**a**) D_A plotted against % net sampled as a function of well array size. Vertical lines link the four different fault cases for each Project. * denotes Project 2 data, which are distinct from the rest of the data because Project 2 models are low net:gross and possess end-member sedimentology. (**b**) and (**c**) Details of (a) for (b) 4 and (c) 16 well arrays, showing the relative positions of the unfaulted and faulted models. Dashed lines link the same models that contain different sets of facies as net, namely Project1[1] and Project1[2] (top right; left and right, respectively), Project2[1] and Project2[2] (bottom, left and right, respectively) and the total model[1] and total model[2] (top middle; right and left, respectively). Note that the 1 m model is the most connected and 'drainable' in all but one Project, even though the equivalent 20 m and 5 m models may be less connected than the unfaulted models (see text for discussion). In all plots, D_A in each case is calculated from the unfaulted models.

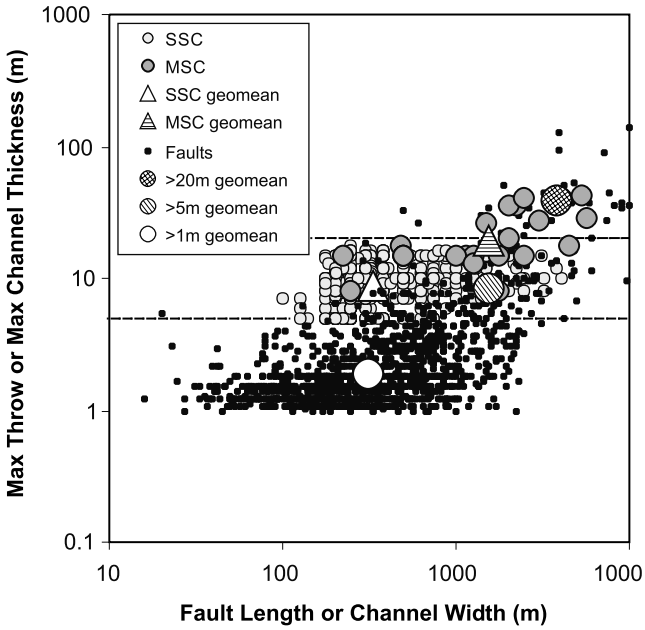

Fig. 17. Relationship between the dimensions of faults and reservoir bodies within the EPC model. Vertical measures (maximum fault throw and channel thickness) are plotted against horizontal measures (fault length and channel width). Individual channels are disconnected when the fault throw is greater than the channel thickness. Similarly, there is a higher probability of faults disconnecting channels when fault length is greater than channel width. SSC and MSC refer to single-storey and multi-storey channels, respectively. Note that overbank deposits are not shown for convenience because of their size (20 000 m wide and 1–2 m thick). The 'geomean' data are the geometric means for the various size distributions.

LIMITATIONS

Our analyses are focused on the geometrical aspects of faulting, with faults acting as hydraulically neutral planes across which reservoir bodies are juxtaposed or dissected. This is a gross simplification, especially for faults within the low net:gross successions of the Coal Measures which are often characterized by fault rocks consisting of clay gouges. Nevertheless, our procedure allows assessment of across-fault reservoir juxtaposition and is a useful prelude to studies of fault seal (e.g. Allan 1989; Bouvier *et al.* 1989; Bentley & Barry 1991; Knipe

1997; Yielding *et al.* 1997) and the impact of faults on reservoir flow (e.g. Walsh *et al.* 1998). Our approach isolates, and therefore allows analysis of, the potential impact of faults on the 3D geometrical connectivity of clastic successions.

Another limitation in our analyses is the detailed representation of faults in cellular models. Faults are geometrically complex structures at scales below the resolution of our cellular models (i.e. 100 m). Different across-fault juxtaposition geometries can arise depending on whether displacement is partitioned onto one or a number of fault segments (e.g. Childs *et al.* 1997; Hesthammer & Fossen 2000). Fault zone complexity on a scale of less than *c.* 100 m cannot be represented in the cellular models presented here and all faults within a single cell (100 × 100 m) must be collapsed onto one structure and their throws aggregated. Although most large displacement faults in the study area are dominated by a single fault segment on scales below 100 m, smaller displacement faults (*c.*<5 m) sometimes form segmented discontinuous arrays. This scale of segmentation would only serve to further increase the connectivity arising from the presence of small displacement faults (i.e. Figs 16b and 16c) and the basic changes in connectivity due to faulting are preserved.

DISCUSSION

We have examined the geometric effects of faults of different sizes on the 3D connectivity of reservoir bodies within low net:gross fluvio-deltaic successions of the British Coal Measures. The population of faults includes faults with maximum displacements down to 1 m and therefore extends well below the limit of resolution of most oil field seismic datasets, which is rarely better than *c.* 20 m displacement. Our analysis suggests that the effects of seismically imaged faults (>20 m displacement) on reservoir connectivity can differ markedly from those of sub-seismic faults. For example, small-scale faulting (i.e. <5 m) can increase bulk reservoir connectivity by reconnecting parts of the reservoir system that are disconnected by larger scale faults (Figs 16b and 16c). This change in connectivity effects can be linked to the relative scaling properties of faults and reservoir bodies.

A crucial issue however is the extent to which geometric connectivity can be linked to fluid flow. Previous work has shown that fault zones within the low net:gross, clastic successions of the British Coal Measures often contain high clay content fault zones, arising from clay smearing and the formation of clay gouges (Lindsay *et al.* 1993; Childs *et al.* 1997). High clay content fault rocks are known to have relatively high capillary entry pressures and relatively low permeabilities (e.g. Fisher & Knipe 2001). By contrast, faults contained within individual sandstones or within sandstone-dominated successions comprise sandstone cataclasites and breccias. The hydraulic properties of these types of fault rocks within Coal Measure successions have yet to be quantified, though unpublished studies suggest that they have higher permeabilities and lower entry pressures than clay rich fault rocks (Childs 2000).

The effect of fault-related geometric connectivity on hydrocarbon migration is two-fold. On the one hand, seismically imageable faults may compartmentalize thicker reservoir units (>20 m), a feature which should be quantifiable from conventional sub-surface data using a range of existing methods (e.g. Bouvier *et al.* 1989; Gibson 1994, 1998; Fulljames *et al.* 1997; Yielding *et al.* 1997). On the other hand, faults with smaller displacements (<20 m), although locally compartmentalizing thinner reservoir units would accentuate vertical migration by the generation of relatively tortuous cross-fault migration pathways, involving the lateral and upward migration of hydrocarbons, as described by Allan (1989).

The changes in connectivity arising from the introduction of faults will have a direct impact on the K_v/K_h ratio of the system at the reservoir scale. Any increase in the connectivity of this multi-layered succession will increase the effective K_v of the system, because flow through thinner fault zones represent more efficient flow pathways than flow through thicker and more persistent low permeability shale units. The increase in K_v/K_h ratio is accentuated by a concomitant decrease in K_h, arising from the lateral compartmentalization of reservoir units. The extent and nature of any increases in K_v/K_h arising from the introduction of faults will therefore depend on a complex interplay between the geometric effects of faults, the nature of the faulted succession and the fault properties. It is very likely that changes in K_v/K_h will be strongly case specific and will require full-field flow simulations of individual systems. Flow modelling of this study area is ongoing and will be the subject of a future companion paper.

CONCLUSIONS

- A high quality 3D faulted stratigraphic cellular model for a *c.* 600 m Westphalian succession from the Carboniferous East Pennine Coalfield provides a basis for examining the effects of faults on the connectivity of reservoir bodies within a delta-top/fluvial reservoir analogue.
- Interval net:gross and the dimensionality of reservoir bodies are the critical determinants in controlling fault-related connectivity changes.
- Faults generally lead to a decrease in connectivity for successions comprising more channelized units. Conversely, successions comprising more tabular sedimentary units generally show an increase in connectivity with the introduction of faults.
- The effects of faults of different size (e.g. seismically imaged v. sub-seismic faults) are sensitive to the relative scales of faults and of sedimentary bodies. Faults with maximum displacements above 20 m (i.e. those which are seismically resolvable from good quality seismic datasets) can result in either an increase or a decrease in reservoir connectivity. Faults with maximum displacements below 5 m (i.e. those which are sub-seismic even for good quality seismic datasets) can significantly increase connectivity even in cases where larger faults, on their own, reduce connectivity.
- The results presented are for a low net:gross (<0.27) Coal Measure succession and are not routinely applicable to other reservoir sequences. Nevertheless, they highlight the potential effects of faults on reservoir connectivity and the requirement to incorporate, or consider, these effects in reservoir characterization and modelling studies.

This work arises from a collaborative research project between the Fault Analysis Group, The Stratigraphy Group and International Mining Consultants and was funded by Exxon Mobil, Japanese National Oil Corporation, Statoil, Texaco and TotalFinaElf. Our thanks are expressed to these companies and their representatives for their support and permission to publish. We thank Roxar for the provision of the RMS/STORM suite of software, which has underpinned our modelling efforts. Two anonymous referees are thanked for their comments.

REFERENCES

Allan, U.S. 1989. Model for hydrocarbon migration and entrapment within faulted structures. *American Association of Petroleum Geologists Bulletin,* **73**, 803–811.

Badley, M.E., Freeman, B., Roberts, A.M., Thatcher, J.S., Walsh, J.J., Watterson, J. & Yielding, G. 1990. Fault interpretation during seismic interpretation and reservoir evaluation. *Proceedings of the 1st Archie Conference: the integration of geology, geophysics, petrophysics and petroleum engineering in reservoir delineation, description and management.* AAPG, Houston, Texas, 224–241.

Bentley, M.R. & Barry, J.J. 1991. Representation of fault sealing in a reservoir simulation: Cormorant block IV UK North Sea. *66th Annual Technical Conference and Exhibition of the Society of Petroleum Engineers, Dallas, Texas*, 119–126.

Bouvier, J.D., Kaars-Sijpesteijn, C.H., Kluesner, D.F., Onyejekwe, C.C. & Van Der Pal, R.C. 1989. Three-dimensional seismic interpretation and fault sealing investigations, Nun River Field, Nigeria. *American Association of Petroleum Geologists Bulletin,* **73**, 1397–1414.

Childs, C. 2000. *The structure and hydraulic properties of fault zones.* PhD thesis. University of Liverpool.

Childs, C., Walsh, J.J. & Watterson, J. 1997. Complexity in fault zones and implications for fault seal prediction. *In:* Møller-Pedersen, P. & Koestler, A.G. (eds) *Hydrocarbon Seals: Importance for Exploration and Production.* Norwegian Petroleum Society (NPF), Special Publication, **7**. Elsevier, Amsterdam, 61–72.

Fisher, Q.J. & Knipe, R.J. 2001. The permeability of faults within siliciclastic petroleum reservoirs of the North Sea and Norwegian Continental Shelf. *Marine and Petroleum Geology,* **18**, 1063–1081.

Fraser, A.J. & Gawthorpe, R.L. 1990. Tectono-stratigraphic development and hydrocarbon habitat of the Carboniferous in northern England. *In:* Hardman, R.F.P. & Brooks, J. (eds) *Tectonic Events Responsible for Britain's Oil and Gas Reserves.* Geological Society, London, Special Publications, **55**, 49–86.

Fulljames, J.R., Zijerveld, L.J.J. & Franssen, R.C.M.W. 1997. Fault seal processes: systematic analysis of fault seals over geological and production time scales. *In:* Møller-Pedersen, P. & Koestler, A.G. (eds) *Hydrocarbon Seals, Importance for exploration and production.* Norwiegian Petroleum Society (NPF), Special Publication, **7**. Elsevier, Amsterdam, 51–59.

Gauthier, B.D.M. & Lake, S.D. 1993. Probabilistic modelling of faults below the limit of seismic resolution in the Pelican Field, North Sea, offshore U.K. *American Association of Petroleum Geologists Bulletin,* **77**, 761–777.

Gibson, R.G. 1994. Fault zones seals in siliciclastic strata of the Columbus Basin, offshore Trinidad. *American Association of Petroleum Geologists Bulletin,* **78**, 1372–1385.

Gibson, R.G. 1998. Physical character and fluid-flow properties of sandstone-derived fault zones. *In:* Coward, M.P., Daltaban, T.S. & Johnson, H. (eds) *Structural Geology in Reservoir Characterisation.* Geological Society, London, Special Publications, **127**, 83–97.

Goossens, R.F. & Smith, E.G. 1973. The stratigraphy and structure of the upper Coal Measures in the Yorkshire coalfield between Pontefract and south Kirkby. *Proceedings of the Yorkshire Geological Society,* **39**, 487–514.

Graham, S. 1988. Structural elements of the Yorkshire Coalfield with particular reference to Selby and the eastern Coal Measures. British Coal, Internal Report.

Hesthammer, J. & Fossen, H. 2000. Uncertainties associated with fault sealing analysis. *Marine and Petroleum Geology,* **6**, 37–45.

King, P.R. 1990. The connectivity and conductivity of overlapping sand bodies. *In:* Buller, A.T., Berg, E., Hjelmeland, O., Kleppe, J., Torsæter, O. & Aasen, J.O. (eds) *North Sea Oil and Gas Reservoirs II.* Graham & Trotman, London, 353–362.

Knipe, R.J. 1997. Juxtaposition and seal diagrams to help analyze fault seals in hydrocarbon reservoirs. *American Association of Petroleum Geologists Bulletin,* **81**, 187–195.

Lia, O., Omre, H., Tjelmeland, H., Holden, L. & Egeland, T. 1997. Uncertainties in Reservoir Production Forecasts. *American Association of Petroleum Geologists Bulletin,* **81**, 775–802.

Lindsay, N.G., Murphy, F.C., Walsh, J.J. & Watterson, J. 1993. Outcrop studies of shale smears on fault surfaces. *In:* Flint, S. & Bryant, A.D. (eds) *The Geological Modelling of Hydrocarbon Reservoirs and Outcrop.* International Association of Sedimentologists Publication, **15**, 113–123.

Manzocchi, T., Walsh, J.J., Nell, P. & Yielding, G. 1999. Fault transmissibility multipliers for flow simulation models. *Petroleum Geoscience,* **5**, 53–63.

Manzocchi, T., Walsh, J.J., Heath, A.E. & Childs, C. 2002. The representation of two phase fault-rock properties in flow simulation models. *Petroleum Geoscience,* **8**, 119–132.

O'Mara, P.T. & Turner, B.R. 1999. Sequence stratigraphy of coastal alluvial plain Westphalian B Coal Measures in Northumberland and the southern North Sea. *International Journal of Coal Geology,* **42**, 33–62.

Omre, H., Sølna, K., Dahl, N. & Tørudbakken, B. 1994. Impact of fault heterogeneity in fault zones on fluid flow. *In:* Aasen, J.O., Berg, E., Buller, A.T., Hjelmeland, O., Holt, R.M., Kleppe, J. & Torsæter, O. (eds) *North Sea Oil and Gas Reservoirs – III.* Kluwer, London, 185–200.

Rippon, J.H. 1985a. Contoured patterns of the throw and hade of normal faults in the Coal Measures (Westphalian) of north-east Derbyshire. *Proceedings of the Yorkshire Geological Society,* **45**, 147–161.

Rippon, J.H. 1985b. New methods of forecasting the throw and hade of faults in some North Derbyshire Collieries. *Transactions of the Institute of Mining Engineers,* **145**, 198–204.

Rippon, J.H. 1997. *Variations in tectonic style and setting in British coalfields.* PhD thesis. University of Keele.

Rippon, J.H. 2000. The Westphalian A to mid-C of Great Britain: new conceptual modelling for hydrocarbon reservoir analogues. *Zentralblatt für Geologie und Paläontologie,* **1**, 217–231.

Sassi, W., Livera, S.E. & Caline, B.P.R. 1992. Quantification of the impact of sub-seismic scale faults on Cormorant block IV. *In:* Larsen, R.M., Brekke, H., Larsen, B.T. & Talleraas, E. (eds) *Structural and tectonic modelling and its application to petroleum geology.* Norwegian Petroleum Society (NPF), Special Publication, **1**. Elsevier, Amsterdam, 355–364.

Walsh, J.J. & Watterson, J. 1988. Dips of normal faults in British Coal Measures and other sedimentary sequences. *Journal of the Geological Society, London,* **145**, 859–873.

Walsh, J.J., Watterson, J. & Yielding, G. 1994. Determination and interpretation of fault size populations: procedures and problems. *In:* Aasen, J.O., Berg, E., Buller, A.T., Hjelmeland, O., Holt, R.M., Kleppe, J. & Torsæter, O. (eds) *North Sea Oil and Gas Reservoirs – III.* Kluwer, London, 141–155.

Walsh, J.J., Watterson, J., Heath, A.E. & Childs, C. 1998. Representation and scaling of faults in fluid flow models. *Petroleum Geoscience,* **4**, 241–251.

Watterson, J., Walsh, J.J., Gillespie, P.A. & Easton, S. 1996. Scaling systematics of fault sizes on a large scale range fault map. *Journal of Structural Geology,* **18**, 199–214.

Yielding, G., Freeman, B. & Needham, D.T. 1997. Quantitative fault seal prediction. *American Association of Petroleum Geologists Bulletin,* **81**, 897–917.

Received 22 January 2002; revised typescript accepted 22 May 2002.